Soft Matter

PAPER

View Article Online
View Journal | View Issue

Cite this: *Soft Matter*, 2015, 11, 8789

Hydrophobic nanoparticles promote lamellar to inverted hexagonal transition in phospholipid mesophases†

Jennifer M. Bulpett,[a] Tim Snow,[a] Benoit Quignon,[a] Charlotte M. Beddoes,[a] T-Y. D. Tang,[a] Stephen Mann,[a] Olga Shebanova,[b] Claire L. Pizzey,[b] Nicholas J. Terrill,[b] Sean A. Davis[a] and Wuge H. Briscoe*[a]

Received 10th July 2015,
Accepted 14th September 2015

DOI: 10.1039/c5sm01705j

www.rsc.org/softmatter

This study focuses on how the mesophase transition behaviour of the phospholipid dioleoyl phosphatidylethanolamine (DOPE) is altered by the presence of 10 nm hydrophobic and 14 nm hydrophilic silica nanoparticles (NPs) at different concentrations. The lamellar to inverted hexagonal phase transition (L_α–H_{II}) of phospholipids is energetically analogous to the membrane fusion process, therefore understanding the L_α–H_{II} transition with nanoparticulate additives is relevant to how membrane fusion may be affected by these additives, in this case the silica NPs. The overriding observation is that the H_{II}/L_α boundaries in the DOPE p–T phase diagram were shifted by the presence of NPs: the hydrophobic NPs enlarged the H_{II} phase region and thus encouraged the inverted hexagonal (H_{II}) phase to occur at lower temperatures, whilst hydrophilic NPs appeared to stabilise the L_α phase region. This effect was also NP-concentration dependent, with a more pronounced effect for higher concentration of the hydrophobic NPs, but the trend was less clear cut for the hydrophilic NPs. There was no evidence that the NPs were intercalated into the mesophases, and as such it was likely that they might have undergone microphase separation and resided at the mesophase domain boundaries. Whilst the loci and exact roles of the NPs invite further investigation, we tentatively discuss these results in terms of both the surface chemistry of the NPs and the effect of their curvature on the elastic bending energy considerations during the mesophase transition.

Introduction

Lipids can self-assemble in water to form a variety of mesophases with different three dimensional structures and molecular arrangements. There has been much research on these mesophase structures in a range of areas including drug delivery,[1] model cell membranes[2] and gene therapy applications.[3] For instance, lipids can be incorporated into solid devices to regulate the absorption of water-soluble drugs to achieve sustained and controlled drug release.[1] In addition, bicontinuous cubic phases have the ability of transporting, both, hydrophobic or hydrophilic drugs by dissolution into the lipid or water region respectively. Structurally, the fluid (L_α) and gel (L_β) lamellar phases formed by lipids are comparable to the cell membrane and are therefore exploited as model cell membranes.[2] The inverted hexagonal (H_{II}) phase formed by DNA–lipid complexes[4] has been suggested as a potential vector for delivering DNA into a cell for gene therapy applications,[3] in a mechanism not dissimilar from that employed by a virus.[5] All of these current and potential lipid mesophase applications depend on our understanding of, and our ability to control, the structures of the mesophases that lipids self-assemble to form.

A number of techniques have been employed to study lipid mesophases. Small-angle X-ray scattering (SAXS) is a key method for identifying liquid crystalline phases and for gaining quantitative information about the length scale of mesophase structures. Efficient and accurate identification of a particular mesophase can be carried out from the relative peak positions present in the SAXS scattering intensity *vs.* Q curve.[6] Here, $Q = (4\pi/\lambda)\sin(2\theta/2)$ is the momentum transfer, with λ the wavelength of the X-ray and 2θ the scattering angle. The various phases are readily identifiable by the fingerprint X-ray scattering patterns which have peak positions in Q, in Q of $1:2:3:4\ldots$ for L_α and $1:\sqrt{3}:2:\sqrt{7}:5\ldots$ for H_{II}. Rheological measurements have also been used to study the structure of a bulk mesophase and its relaxation properties. For instance, Mezzenga *et al.*[7] have previously shown that each mesophase has a particular shear rheological signature in a study of the lipid monolinolein.

[a] *School of Chemistry, University of Bristol, Cantock's Close, Bristol BS8 1TS, UK. E-mail: wuge.briscoe@bris.ac.uk; Tel: +44 (0)117 3318256*
[b] *Diamond Light Source Ltd, Diamond House, Harwell Science and Innovation Campus, Didcot, OX11 0DE, UK*

† Electronic supplementary information (ESI) available. See DOI: 10.1039/c5sm01705j

Furthermore, cryo-transmission electron microscopy (Cryo-TEM) can be used to visualise the structure of mesophases.[8–10]

The exact mesophases that a particular lipid will form depends on a number of factors: those specific to the lipid itself including its molecular volume, hydrophobic chain length and headgroup area at the hydrocarbon–water interface, and other factors related to its environment such as hydration, pH, temperature and pressure.[11] Therefore, to access different phases of a particular lipid for different applications, the temperature, pressure and hydration can be altered to control both the lipid self-assembly process and the resultant mesophase morphology. Additives such as a second lipid,[10,11] cholesterol,[12,13] surfactants[14] and nanoparticles (NPs)[9,15] can also be used to tune mesophase behaviour, subtly and judiciously. For instance, nanocomposites[16] are hybrid three-dimensional materials formed from a combination of NPs and self-assembling molecules such as copolymers or lipids. Addition of NPs to these self-assembling molecules will affect the overall molecular structure of the lipid and co-polymer, thus altering the phase behaviour in comparison to the pure lipid. For example, mixed liposomes of the phospholipid dioleoyl-*sn-glycero*-phosphocholine (DOPC) and CdTe NPs were formed[17] and then deposited on a hydrophilic surface yielding a lamellar liquid crystalline nanocomposite structure with NPs located within the hydrophilic regions. NPs also affect similar but non-lipid systems; *e.g.* it has been shown that AOT mesophases containing silver nanoparticles[18] can introduce useful physicochemical and optical properties. Therefore, the understanding of the effects of NPs on mesophase behaviour is vitally important for the rational design of these nanocomposites.

The L_α–H_{II} and L_α–Q_{II} mesophase transitions are of particular interest in biology because the molecular deformations experienced by lipid molecules during these transitions have been predicted to be comparable to the low energy structural intermediates of membrane fusion, which occurs in processes such as endocytosis.[19,20] The energetics of which are described in the stalk model of membrane fusion. The process begins with stacked lipid bilayers in the L_α phase making initial point contacts, often by dehydration of the lipid headgroups. These contacts merge and develop into a stalk intermediate. The distal monolayers subsequently nipple in to form the transmonolayer contact (TMC), which expands radially, finally leading to pore formation. The intermediate steps between L_α and Q_{II} or L_α to H_{II} are comparable to intermediates in the stalk mechanism.

Such a membrane fusion process is also relevant to the membrane crossing process by NPs.[20] The cell membrane is composed of a phospholipid bilayer embedded with other biomolecules, such as proteins and cholesterol. The L_α phase formed by phospholipid–water mixtures has been used as simple model systems for cell membranes in order to study the process of membrane fusion by methods including SAXS.[19] Many reviews[20–25] have highlighted the importance of fundamental understanding of nanotoxicity, and they emphasise that whilst phenomenological studies of cells and NPs give some indication of whether a particular NP is toxic or not, little is known of the complex physical mechanisms of how NPs impart toxicity. In the majority of cases of NP toxicity and for therapeutic NP use, the NPs would gain cellular entrance. In order to do so, they would first interact with the membrane, which would lead to local deformations and eventual cellular entrance *via* the endocytosis mechanism. Based on the above energetic analogy between mesophase transitions and cell membrane fusion, this study aims to investigate the effect of the presence of silica NPs on the lipid L_α–H_{II} phase transitions by utilising the phospholipid (DOPE)–water mixture as a simple model system. Typically, the cell membrane consists of a phospholipid bilayer within which are embedded other biomolecules, such as proteins and cholesterol.[19] We aim to improve our fundamental understanding of the correlation between the physical parameters that characterise NPs (*e.g.* size, dosage and surface chemistry[26]) and their ability to gain cellular entrance.

Mesophase transitions (such as L_α–H_{II} that we are interested in) can be readily induced by varying the hydration level and temperature of a lipid–water mixture, as commonly employed in many studies.[27–31] In addition, this phase transition can be induced by varying the pressure applied to the mesophase,[11] as utilised in this study. The thermodynamic effect of pressure is described by Le Châtelier's principle,[32] which in this context states that with increasing pressure a system will shift its equilibria to the state that occupies the least amount of space as the system attempts to minimise the effect of the pressure increase. Consequently at high pressures, mesophases with a smaller volume (such as gel phases) prevail, and phase transitions involving an intermediate phase with a volume smaller than the initial phase are encouraged.[33] The effect of pressure on the lipid bilayer micromechanics can be appreciated by considering the curvature elastic energy, which for a lipid monolayer[34,35] is given as $g_c = 2\kappa(H - H_0)^2 + \kappa_G K$, where g_c is the curvature elastic energy per unit area, $H = (c_1 + c_2)/2$ the mean curvature and $K = c_1c_2$ the Gaussian curvature, with c_1 and c_2 the principle curvatures of the surface, H_0 the spontaneous mean curvature, and κ and κ_G are the mean and Gaussian curvature elastic moduli, respectively. As discussed in a recent paper, it is pertinent to consider the effects of pressure on the pivotal surface (surface from which the energy is measured from), and ultimately, pressure affects the lateral stress profile which underpins the changes in the curvature elastic energy.[36]

As previously discussed by Brooks *et al.*[37] in lipid systems, an increase in pressure has the opposite effect to increasing temperature qualitatively.[38] An increase of pressure constrains the movement of the tail and so increases ordering of the tail region and reduces the cross-section of the tail. The headgroup is less affected by pressure increase, and so a monolayer will either have an increased curvature towards the tail (*i.e.* a larger curvature) or, if the lipid has a tendency for inverse curvature, the magnitude of the negative spontaneous curvature is decreased. In H_{II} mesophases, the reduction in the volume of the chain and subsequent decrease in negative curvature leads to an increase of the H_{II} lattice parameter[39] and thus an increase of the diameter of the H_{II} cylinders.

As a result, pressure can be employed as an alternative to temperature to induce phase transitions[11] and in fact this approach

bears numerous advantages, such as a decrease of the equilibration time as the pressure propagates instantaneously through the sample,[40] thus allowing kinetic studies of the mesophase transition which would not be possible with temperature due to much longer equilibrium time required. The solvent properties are also unaffected by alteration of pressure. The overall effect of pressure on the lipid transition temperature, T_t, can be calculated at phase boundaries utilising the *Clapeyron* equation:[37]

$$\frac{dT_t}{dp} = \frac{\Delta V_m}{\Delta S_m} = \frac{T_t \Delta V_m}{\Delta H_m} \quad (1)$$

where ΔS_m, ΔH_m and ΔV_m are the molar transition entropy, enthalpy and volume changes, respectively. This relationship is linear if ΔS_m and ΔV_m are independent of pressure or have similar pressure dependence[37] as ΔH_m is endothermic.[11]

In this paper, dioleoyl phosphatidylethanolamine (DOPE) lipid model systems have been used, as its mesophase behaviour has been well characterised both by varying temperature and water content,[28] and by varying temperature and pressure[11] with a wide range of techniques such as nuclear magnetic resonance (NMR),[41] X-ray diffraction[41] and differential scanning calorimetry (DSC).[28] The pressure–temperature (p–T) phase diagram of pure DOPE in excess water has been obtained by Winter[11] with SAXS. Briefly, the H_{II} phase is present in the top left region of the p–T phase diagram at temperatures greater than 10 °C and at low pressures (below 1800 bar), bordered by the L_α phase at intermediate temperatures (from −10 °C at low pressure to over 60 °C at higher pressures) and in the full pressure range shown. The L_c phase is formed at the highest pressures and lower temperatures and does not occur above 20 °C in the pressure range probed. DOPE has a propensity for forming the H_{II} phase,[41] due to its inherent molecular shape (*cf.* Fig. 1) with a relatively smaller headgroup compared to the lamellar-forming lipid dioleoyl phosphatidylcholine (DOPC). For this reason, DOPE has been utilised to dope DOPC membranes in order to introduce curvature and consequently, the ribbon phase has been stabilised in this way.[12] A study by Chen *et al.*[42] has examined the effect of cholesterol and tetradecane on the curvature and elasticity of DOPE in systems containing tetradecane with XRD and osmotic stress measurements. DOPE formed the H_{II} phase both with and without added cholesterol, where cholesterol was shown to decrease the radius of the intrinsic curvature from 29.4 Å to 27 Å with 30% cholesterol. The addition of tetradecane had little effect on DOPE and DOPE/cholesterol systems. Mixtures of DOPE with DNA have also been studied with freeze-fracture transmission electron microscopy (TEM) for its use as potential drug delivery vectors[3] and it was observed that different structures were formed dependent on the quantity of DNA and incubation time of the mixture.

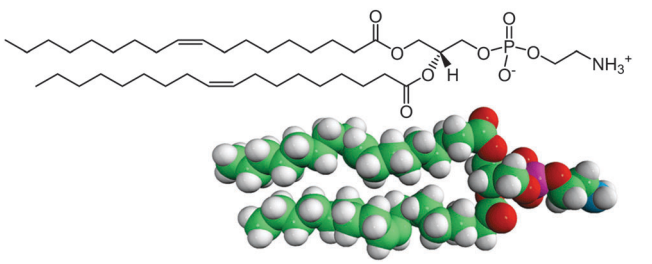

Fig. 1 Structure and space-filling 3D model of DOPE.

In this study, silica NPs were selected as their applications and their cytotoxicity has been widely documented. Furthermore, the potential and current uses of silica NPs are numerous, including drug delivery and gene transfection,[43] bioconjugation and biomarkers,[26,44] Related toxicity studies include the effect of functionalized silica NPs on endocytosis in human cancer cells,[45] where more negatively charged NPs were shown to escape from endosomes at a faster rate and the uptake of NPs was shown to be dependent on their surface functionalisation. A study using silica NPs of a broad range of sizes varying from 2 nm to 335 nm by Thomassen *et al.*[46] showed that the cytotoxic effects were dependent not only on the cell type but also the NP size, with smaller NPs being more toxic. Another study by Slowing *et al.*[43] found that their mesoporous silica nanoparticles could have potential drug delivery applications due to their biocompatibility, with cell tests showing no decreased proliferation or viability on mammalians cells after 7 cell cycles.

For the model systems of NP–lipid mixtures, DOPE (with excess water) and silica NPs have been used. This experimental design exploits the conjecture that L_α to H_{II} phase transition is energetically analogous to the membrane fusion event occurring during endocytosis.[31] The phase transitions have been induced by altering both pressure and temperature and were examined using SAXS. The mesophase phase transitions have been compared between systems with and without silica NPs of two different surface coatings (*i.e.* hydrophobic and hydrophilic). The aims of this paper are to establish how the phase boundaries are affected by the addition of NPs and how the properties of the NPs and their concentration influence the mesophase transitions. It is found that the hydrophobic NPs had a greater effect of DOPE phase behaviour where L_α–H_{II} phase transition took place at lower pressure compared to pure DOPE.

Results and discussions

From the results collected, seven pressure–temperature (p–T) phase diagrams were produced (*cf.* Fig. 2 and 3) in the range p = 1–3000 bar and T = 20–45 °C, and each data point (✦) in the phase diagrams represents a measurement. In general, different samples exhibited H_{II}, L_α and L_c phases in different T and p ranges. For most samples, their phase was facile to assign from the peak Q ratios. Along the boundary between the H_{II} and L_α phase regions, however, there was a region of L_α–H_{II} phase coexistence as previously reported in the literature.[29] These points were designated as "L_α–H_{II} mixed". As a control, the first phase diagram produced was that of DOPE in excess water (without nanoparticles; *cf.* Fig. 2). Example 2D scattering patterns for four specific data points on the p–T phase diagram respectively from four phase regions for the control sample are shown in Fig. 2, with corresponding schematic mesophase

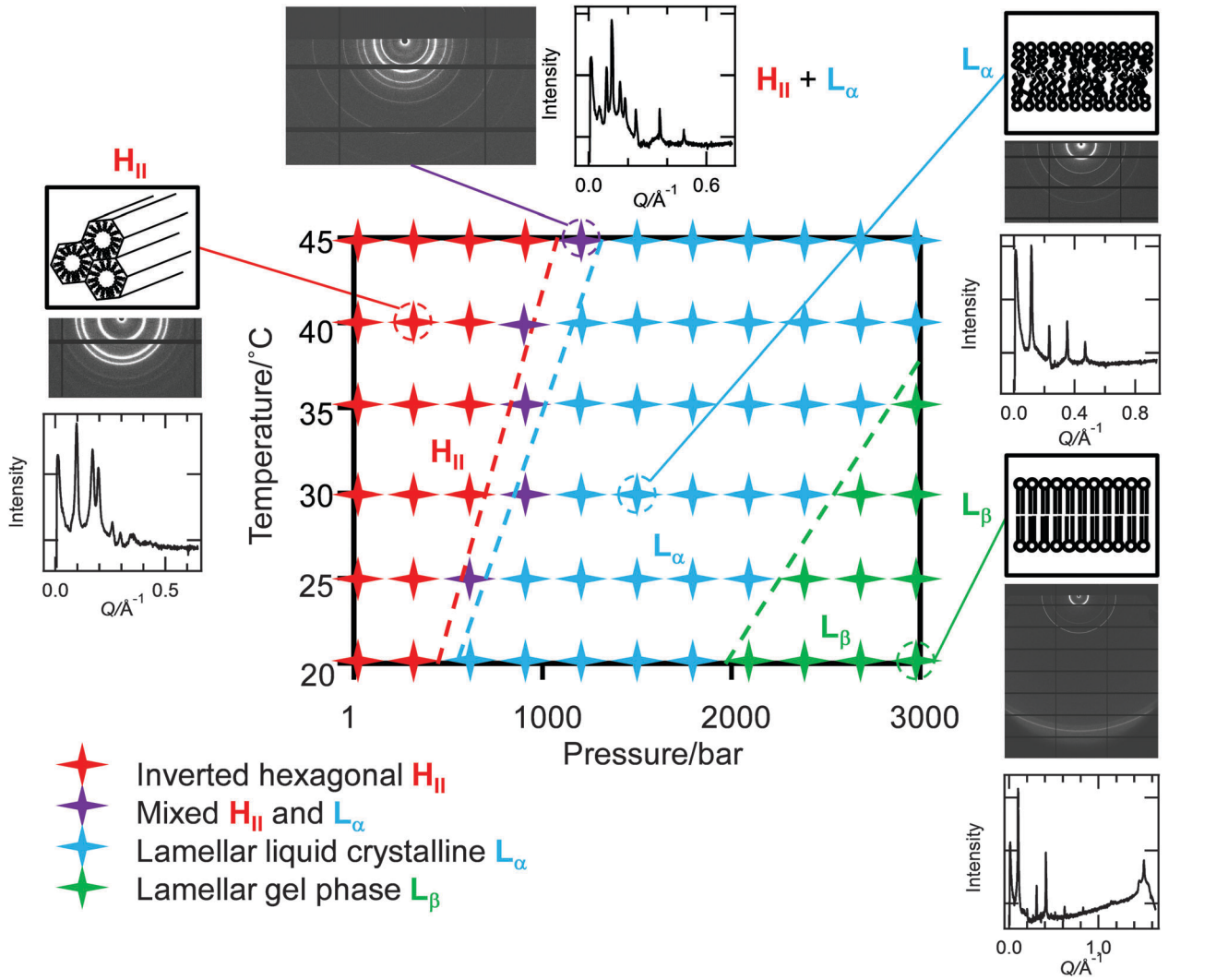

Fig. 2 p–T phase diagram for the control sample (without NPs) showing representative 2D diffraction patterns and corresponding integrated 1D curves for the encircled specific data points.

structure and radially integrated 1D intensity graphs (*i.e. I vs. Q*) also shown.

This control phase diagram is largely consistent with that previously reported in the literature by SAXS,[11] with the exception of a small region at the L_α–H_{II} boundary, where we have observed a region of L_α–H_{II} coexistence. We attribute this to possible differences in sample preparation and equilibration time allowed for the samples, or potentially due to measuring at small pressure intervals which allowed us to see this thin phase coexistence region. It should be noted that all our samples have been prepared consistently using the same procedure and our subsequent SAXS measurements with added NPs have been performed under conditions identical to those for the control sample in Fig. 2.

The other six phase diagrams (Fig. 3) were produced from samples which contained either hydrophilic SiO_2NPs of 14 nm in diameter or hydrophobic SiO_2NPs of 10 nm in diameter mixed with the DOPE at NP-to-lipid number ratios ν = 10^{-6}, 10^{-5} and 10^{-4}, corresponding to NP-to-lipid volume ratios $f_v \cong 1.16 \times 10^{-3}$, 10^{-2}, 10^{-1} respectively. In general, these phase diagrams show that the L_α–H_{II} transition was affected by the presence of NPs, in addition, our results indicate that this effect is also dependant on the surface functionality of the SiO_2NPs as well as the number ratio (ν). We note that the hydrophilic and hydrophobic particles differ in their nominal sizes by 4 nm on average, and the effect of such a size difference would be associated with the curvature related elastic bending energy, should the NPs be individually engulfed by lipid monolayers/bilayers. However, they are both much larger than the d-spacing of the lipid bilayers, and neither of them intercalates into the bilayer structures (see Discussion section below). Their curvatures also differ significantly from the spontaneous curvatures of the mesophases studied here. Our results using hydrophilic AuNPs of ~10 nm in size (to be published) further substantiate that NP surface chemistry indeed plays a prominent role in their interactions with lipid and surfactant mesophases. Nonetheless, we should bear in mind that, when discussing the effect of the NP surface chemistry, it is likely that it is convoluted with other NP physical parameters, such as size, total

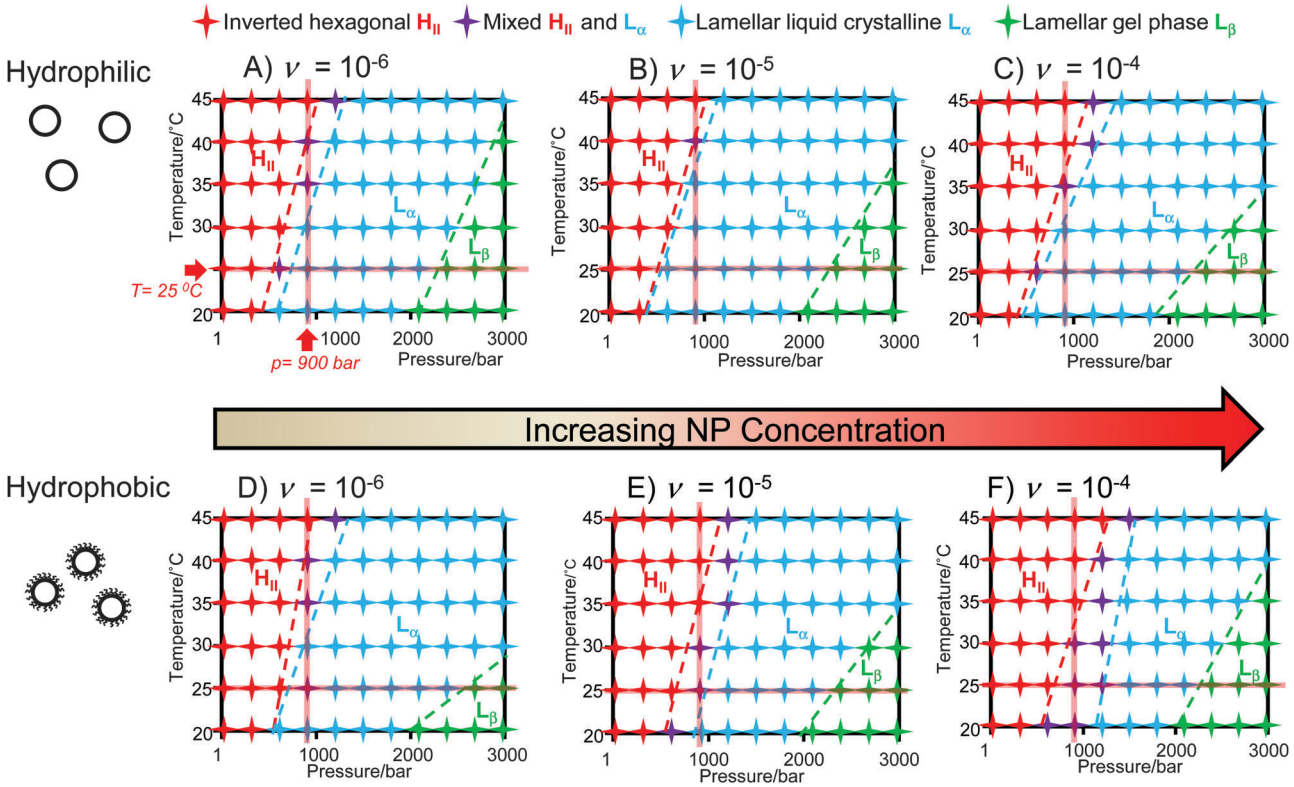

Fig. 3 p–T phase diagrams for the samples containing two types of SiO_2NPs at different NP-to-lipid number ratio ν. In the case of samples with hydrophilic NPs the ν values are: (A) 10^{-6}, (B) 10^{-5} and (C) 10^{-4}, and those with the hydrophobic NPs are (D) 10^{-6}, (E) 10^{-5} and (F) 10^{-4}. The pink horizontal and vertical lines in the figures indicate where T_t and p_t data for Fig. 5 and 6 are taken.

surface area, polydispersity (*cf.* Fig. S2 and S3 in the ESI†), concentration *etc.*

In general, hydrophobic NPs (*cf.* p–T phase diagrams in Fig. 3(D–F)) had a greater effect on the DOPE p–T phase diagram than the hydrophilic NPs (*cf.* p–T phase diagrams in Fig. 3(A–C)) compared to the pure DOPE p–T phase diagram.

Addition of NPs to DOPE mesophases alters the phase behaviour to an extent where the p–T phase diagram has different relative areas of each mesophase region and the boundary positions are altered. This effect is dependent on both the surface coating and concentration of the NPs with differing effects seen for the hydrophobic and hydrophilic NPs. To illustrate the different phase behaviours in these samples due to the addition of the NPs, the relative area (in percentages) pervaded by different phases in the p–T phase diagrams is plotted against ν in Fig. 4(A) (for hydrophilic SiO_2NPs) and Fig. 4(B) (for hydrophobic SiO_2NPs).

There are a number of trends observed as the NP concentration is altered. A small effect is observed in the relative area of each phase in the case of adding hydrophilic SiO_2NPs as compared to the control sample, as shown in Fig. 3(A–C) and 4(A). At ν = 10^{-6}, L_β and L_α–H_{II} mixed regions are slightly promoted, at the expense of the L_α phase, whilst the H_{II} area remains unchanged as compared to the control sample. At $\nu = 10^{-5}$, the L_α phase area is slightly augmented, whilst the H_{II} phase and L_α–H_{II} mixed phase are slightly suppressed. At high NP-to-lipid ratio $\nu = 10^{-4}$, the relative area of each phase almost returns to that in the control sample.

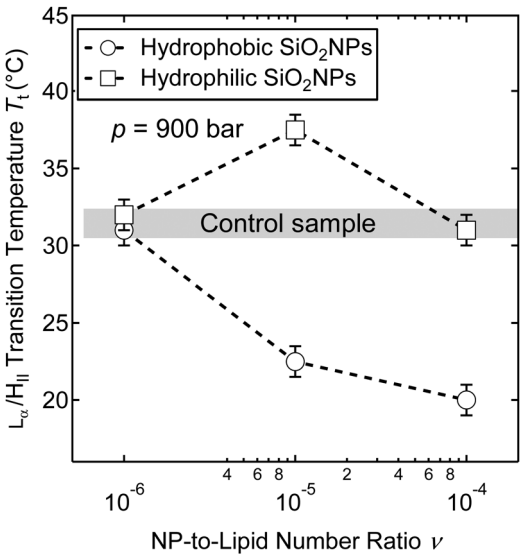

Fig. 4 Temperature at which the H_{II} phase first appears, T_t, at pressure 900 bar as a function of the NP-to-lipid number ratio, ν, as the systems with hydrophilic SiO_2NPs (□) and hydrophobic SiO_2NPs (○) are heated. The corresponding T_t's for the control sample are indicated as the grey horizontal band. The size of the error bars is ±1.0 °C.

It is evident from Fig. 3(D–F) that as hydrophobic NP concentration increases from ν = 10^{-6} to ν = 10^{-4}, the L_α lamellar region (blue) decreases in size whilst the other three

phase regions increase in size, as also shown in Fig. 4(B). At low NP $\nu = 10^{-6}$, the L_α phase area is augmented at the expense of the other lamellar phase, L_β. As the NP ν increases to 10^{-5} and then 10^{-4}, the L_α lamellar phase area is suppressed as compared to the control sample, whilst prominently the inverted hexagonal H_{II} phase region expands.

It is apparent from the results presented here that the addition of hydrophobic silica NPs alters the p–T phase diagram of DOPE, increasing the H_{II} region. This is likely to be due to the presence of NPs encouraging local curvature, which reduces the energy barrier for the L_α to H_{II} phase transition. In contrast, the hydrophilic NPs seem to have the opposite effect, stabilising a larger L_α region at higher NP concentrations than the control sample, indicating that surface chemistry is an important factor as it determines the location of residence of the NP in phase evolution seem to have the opposite effect, stabilising a larger L_α region at higher NP concentrations than the control sample, indicating that surface chemistry is an important factor as it determines the location of residence of the NP in phase evolution.

Fig. 5 plots the phase transition temperature, T_t (*i.e.* the temperature at which the H_{II} phase first appeared upon heating), *vs.*, ν, at $p = 900$ bar. This is indicated with upward red arrows and vertical lines at 900 bar in the p–T phase diagram in Fig. 3, and T_t would be where the line intercepts with the phase boundaries. A clear trend is observed that the temperature for T_t ($L_\alpha \rightarrow$ mixed) for the control sample is $\sim$30 °C as indicated by the grey horizontal band, but this is suppressed to $\sim$20 °C with the highest concentration of hydrophobic NPs, $\nu = 10^{-4}$. We first observe the H_{II} phase in the mixed region meaning the H_{II} phase appeared at lower temperatures in the presence of the hydrophobic SiO_2NPs as compared with the control sample. The effect of hydrophilic NPs on T_t is less clear-cut. As the NP concentration is increased, T_t is elevated as compared to the control sample at $\nu = 10^{-5}$, but is suppressed as compared to the control sample at $\nu = 10^{-6}$ and 10^{-4}. An elevated T_t ($L_\alpha \rightarrow$ mixed) indicates that the hydrophilic NPs stabilised the lamellar phase, in contrast to the destabilising effect of hydrophobic NPs. This is consistent with the observation from Fig. 4(A), which shows that the increase in concentration of hydrophilic NPs leads to a slight increase in the relative area of the L_α phase region and a slight decrease in the L_β phase region in the p–T phase diagram of DOPE, but again this shift from the control sample is less pronounced than that seen with the hydrophobic NPs (*cf.* Fig. 4(B)) (Fig. 6).

As mentioned earlier, the Clapeyron equation predicts that T_t varies with p if ΔS_m and ΔH_m are pressure independent. The slope of the phase boundaries in the phase diagrams (dT_t/dp) has been altered with the addition of NPs in some cases when compared to the control phase diagram. dT_t/dp is typically in the range of 20–30 °C kbar^{-1} for the L_α/H_{II} phase transition of phospholipids and it can also be calculated from DSC and pressure perturbation calorimetry (PPC) to determine ΔH_m and ΔV_m respectively.[40] Specifically for DOPE, dT_t/dp has been found to be 40 °C kbar^{-1} by a combination of SAXS and wide-angle X-ray scattering (WAXS).[33] For all the samples, dT_t/dp for

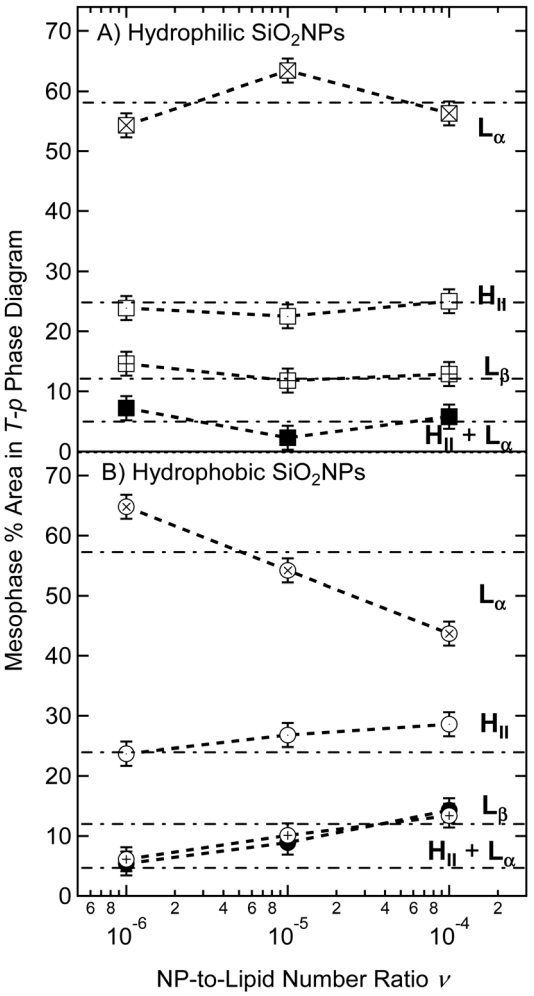

Fig. 5 Relative area of each mesophase (in percentage) in the phase diagrams, for hydrophilic SiO_2NPs (A) and for hydrophobic SiO_2NPs (B). The respective values for the control sample are indicated as horizontal dot-dashed lines. The size of the error bars is ±2%.

the L_α–H_{II} transition is calculated from the boundary between the mixed and H_{II} region and is presented in Fig. 7. The control phase diagram gives a dT_t/dp of 38.9 °C kbar^{-1} which agrees well with the literature value[33] and is shown as a horizontal, dashed line in the figure. With both types of NPs, dT_t/dp decreases with $\tilde{\mu}$ For the hydrophilic SiO_2NPs the dT_t/dp *vs.* ν gradient decreases from 44.8 to 29.4 °C kbar^{-1} and for the hydrophobic SiO_2NPs the slope varies from 62.8 to 33.6 4 °C kbar^{-1}as the NP concentration increases from 10^{-6} to 10^{-4}.

According to the Clapeyron equation (eqn (1)), the thermodynamic effect of NPs on dT_t/dp may be composed of their effects on ΔS_m (or ΔH_m) and ΔV_m (*i.e.* molar transition entropy and volume change respectively). At low NP concentration of $\nu = 10^{-6}$, the interactions between NPs and the lipids dominate and suppress the ΔS_m value, and this entropic term should account for both the additional lipid tail/head – NP interactions and reduced elastic bending energy during the phase transition. At high NP concentration of $\nu = 10^{-4}$, the effect of NPs on ΔV_m dominates; that is, the presence of NPs enhances the

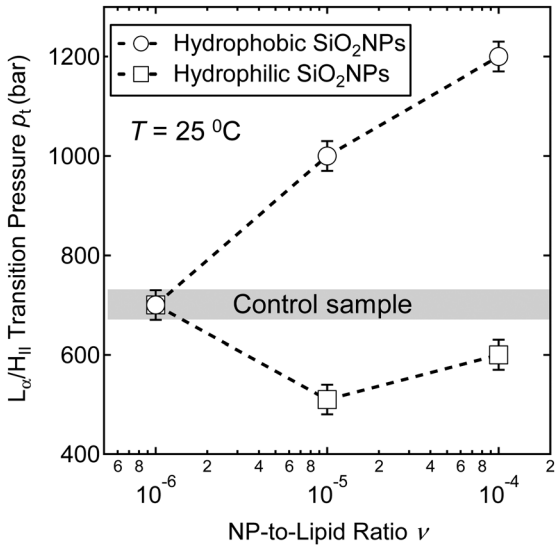

Fig. 6 Pressure at which the H_{II} phase first appears, p_t, *vs.* ν, at a temperature of 25 °C for systems with hydrophilic SiO_2NPs (□) and hydrophobic SiO_2NPs (○). The transition pressure for the control sample is shown as the grey horizontal band. The size of the error bars is ±30 bars.

fluidity of the lipid tails. If the phase transition is a liquid–liquid one then the volume change ΔV_m will be smaller than that for a liquid–gel transition and so T_t is less pressure dependent. At intermediate NP concentration of $\nu = 10^{-5}$, these two effects negotiate a delicate balance.

The above interpretation is qualitative, and further careful calorimetry studies to independently yield ΔS_m, ΔH_m and ΔV_m values would allow it to be evaluated quantitatively. However, this interpretation also has an important implication for the effect of NPs on the structure of the lipid, as the fluidity of the tails is intricately related to ΔV_m and thus to the thickness of the lipid monolayers – which is the fundamental length scale to describe the mesophases.

Venugopal *et al.*[47] studied the phase behaviour of monolinolein, which has a single chain rather than the two of DOPE, with added hydrophilic silica NPs of 5 nm diameter. They found that an increasing concentration of NPs decreased the lattice parameter of the cubic phase and that at higher concentrations the NPs exhibited an independent structure factor peak in the SAXS patterns, which indicated that the NPs were macrophase separated rather than incorporated into the structure and that

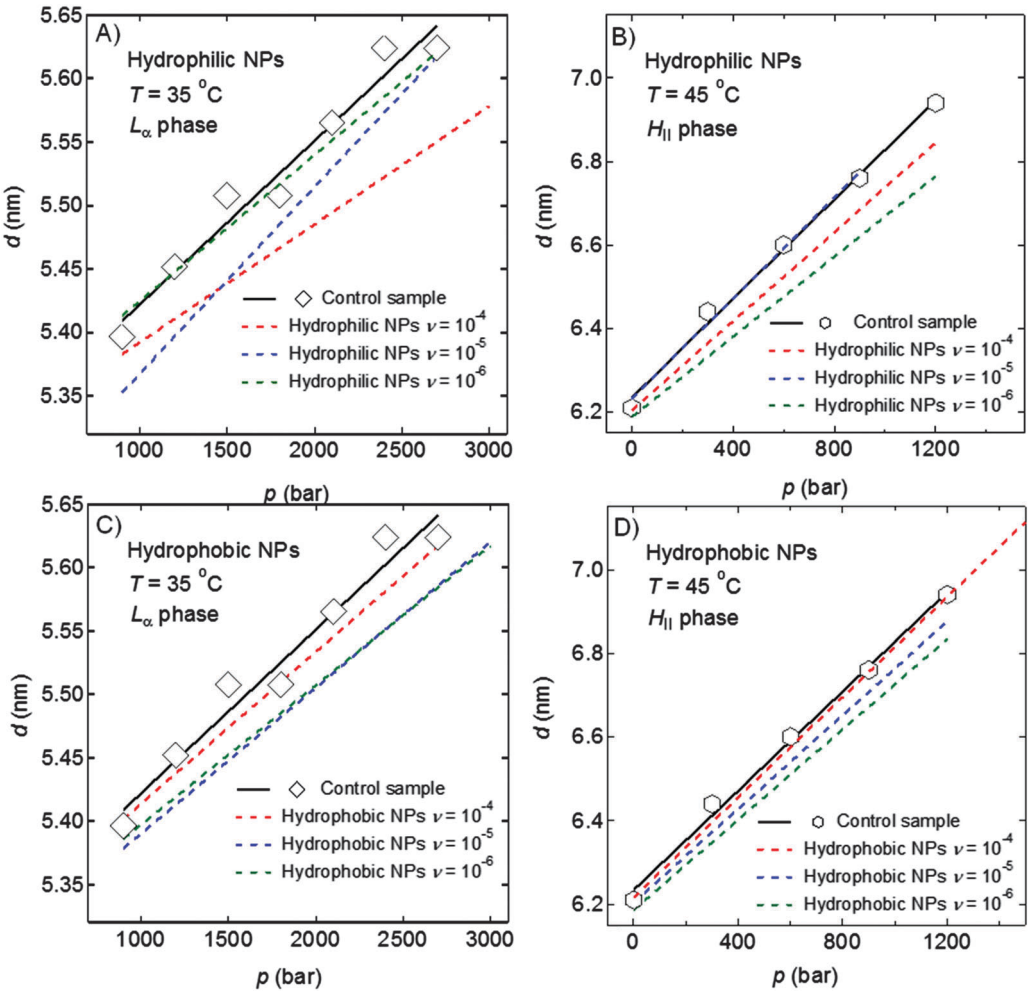

Fig. 7 Pressure dependence of *d*-spacing of the L_α and H_{II} phases for the control sample (without NPs) and for the samples with hydrophilic NPs (A and B) and hydrophobic NPs (C and D). For clarity, only the linear fits to the data points for the samples with NPs are shown. Full data sets are shown in Fig. S1 in the ESI.†

they dehydrated the lipid mesophase by removal of water from lipid head groups to stabilise the NP aggregates. It was also shown that the *Ia3d*(cubic) to H_{II} phase transition temperature decreased with increasing NP concentration. Lower NP concentrations increased the H_{II} *d*-spacing but with higher concentrations the *d*-spacing was reduced as NPs aggregated outside the mesophase. For the L_α phase, lower NP concentration caused swelling of the lamellar layers, and at higher NP concentrations the *d*-spacing was reduced, similar to that seen with the H_{II} phase.

In a study by Chen *et al.*,[18] hydrophobic and hydrophilic NPs were mixed with L_α (sodium) bis(2-ethylhexyl) sulfosuccinate (AOT) and it was found that depending on the surface chemistry and concentration of the NPs, the NPs were located in different positions within the lamellar phase. That is, the hydrophilic NPs were found in the water layer and the hydrophobic NPs in the organic layer. Higher hydrophilic NP concentration caused phase separation, and the hybrid with hydrophilic NPs was more stable than that with both hydrophilic and hydrophobic NPs. Here, we have also observed that the hydrophobic NPs have had a more pronounced effect on the mesophase behaviour than the hydrophilic NPs. It is evident from the *d*-spacing data (*cf.* Fig. 8) that the NPs (of size ~twice that of the mesophase lattice spacing) were not intercalated into the phases, which would have led to a *d*-spacing increase of 10–14 nm.[38] In a previous study[48] it was also found that NPs did not infiltrate purple membranes which had a high protein content and thus a much higher bending modulus than that model lipid membranes. If the NPs phase separated in the sample and formed densely packed and well organised macro-domains, as one would expect for such concentrated regimes, we would expect to observe structure peaks emerge as such macroscopic domains formed. A counter-argument would be that the NPs formed an amorphous structure, but it would be difficult to rationalise the high interfacial energetic cost of voids. In addition, if NPs aggregated in the samples, leading to complete phase separation, we would expect the mesophase characteristics (*e.g.* *d*-spacing and phase transitions) to return to that of the control sample, or not to be influenced significantly by the NP concentration. Fig. 9 shows the how the pressure dependence of the *d*-spacing for the La phase (Fig. 9A) and the H_{II} phase (Fig. 9B) varies with the concentration of the hydrophobic and hydrophilic NPs. Whilst a trend is less clear-cut for the hydrophilic NPs, there is an observable dependence of (d*d*/d*p*) on the NP-to-lipid ratio ν.

Alternatively, we suggest that the NPs could be predominantly located in mesophase domain boundaries, dispersed throughout the sample. It is conceivable that the NPs would be coated with the lipids, either with the lipid tails pointing inward or outwards,

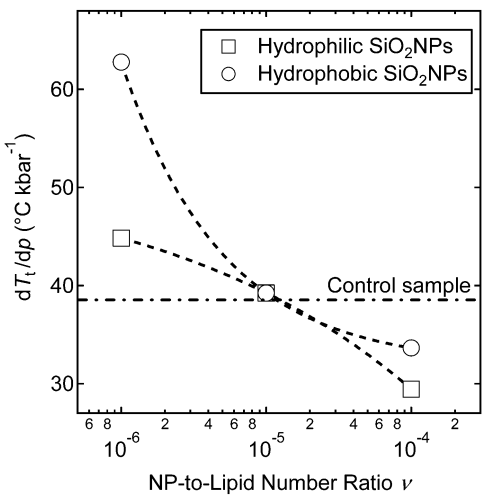

Fig. 8 dT_t/d*p* *vs.* ν for hydrophilic and hydrophobic SiO_2NPs with control sample shown as horizontal dot-dashed line at 38.9 °C kbar^{-1}.

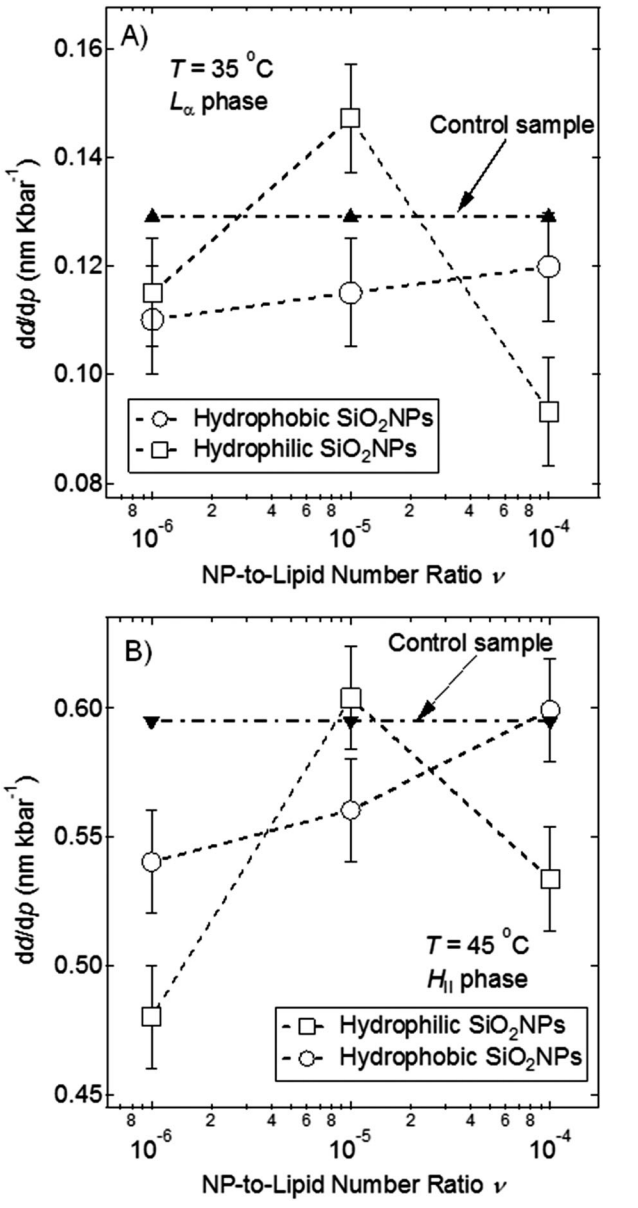

Fig. 9 d*d*/d*p* *vs.* NP-to-lipid number ratio ν for the samples with hydrophilic SiO_2NPs (A; *T* = 35 °C) and hydrophobic SiO_2NPs (B; *T* = 45 °C), as compared to the control sample (no NPs). The size of the error bars is ~±0.1 nm kbar^{-1}.

depending on the NP surface chemistry. Their presence at the domain boundaries would help reduce the high interfacial energy associate with the defects in the lipid packing and possible exposure of hydrophobic tails to the aqueous surroundings. This would also imply that, in the case of hydrophilic silica NPs, pressure could lead to expulsion of water from the mesophase domains, encouraged by the hydrophilic NPs present at domain boundaries. Our current studies with a related system which shows similar behaviour by SAXS will also employ cryo-TEM studies to clarify the location of the particles (Beddoes *et al.* in prep). Further studies could also employ fluorescent particles to help clarify the distribution of the NPs in the sample.

The hydrophobic NPs in this study have been shown to stabilise the H_{II} phase. This broadly agrees with simulation results by Reynwar *et al.*[49] where similar sized, protein nanoparticles ($\sim$10 nm in size) added to a flat membrane were shown to promote local curvature, leading to a fusion pore formation in the membrane. These nanoparticles in effect encouraged the L_α–H_{II} transition, and as discussed earlier, the H_{II} phase has been implicated as an intermediate structure in the fusion pore formation. However, our results also show that hydrophilic NPs of sizes comparable to that of the hydrophobic NPs stabilise the L_α phase. Thus, it is clear that the effect of NPs depends on their surface chemistry as well as their curvature and concentration, all of which affect their overall interactions with the mesophase.

When mixed with the H_{II} phase, it would be energetically favourable to accommodate hydrophobic NPs between domains which are also hydrophobic in nature. Transition to the L_α phase would mean that the hydrophobic NPs are expelled from the hydrophobic environment, an entropically unfavourable process which could be alleviated by adsorption of lipid molecules with their tails down, *i.e.* in contact with the hydrophobic NPs, exposing the head groups. The lipid monolayers thus formed possess a curvature templated by the underlying NPs, which would mismatch that of a bilayer. This process is again energetically unfavourable. As a result, the presence of hydrophobic NPs would stabilise the H_{II} phase, an effect that scales with the NP concentration.

For the hydrophilic NPs to be accommodated in the hydrophobic regions between the H_{II} phase domains, the particles would need to be "hydrophobised" with a monolayer of the lipid molecules, with the tails pointing outwards. However, this process would take place at the expense of unfavourable elastic bending energy; *i.e.* due to the curvature of the NPs mismatching that thermodynamically favoured curvature of the H_{II} cylinders, the elastic bending energy of the NP-adsorbed monolayers would be unfavourable. Upon transition to the L_α phase, the NPs could acquire a second monolayer of lipids to address the entropic disturbance to now hydrophilic inter-domain regions. However, this again would mean the NP-bound bilayers would adopt a thermodynamically unfavoured curvature as templated by the NPs. This elastic bending energy cost is counter balanced to a certain extent by the interactions between the phosphatidylethanolamine (PE) headgroups and the NP silica surface. As such, the effect of the hydrophilic NPs is not as clear-cut. A further consideration is that the hydrophilic NPs may be causing dehydration of the mesophase; however, as the samples were at excess hydration, this is unlikely.

The energetic considerations above are likely to be further complicated by the fact that the interactions between the lipids and both the NPs, either hydrophobic or hydrophilic, would to a certain extent deplete the lipid molecules in the mesophases and thus create structural defects and affect the packing of the lipid molecules, reducing the *d*-spacing and promoting the fluidity of the tails as we have observed. Another simplistic interpretation could be that the presence of the NPs exert an additional osmotic pressure which depends on the NP concentration. However, this does not explain the effect of the NP surface chemistry. As such, understanding the effects of NPs on lipids mesophase transitions should take into considerations the multifarious aspects of NP–lipid interactions and the overall energetic cost associated with the NP curvature.

Conclusions

Using high pressure SAXS, we studied the pressure–temperature (*p*–*T*) DOPE mesophase behaviour, and in particular H_{II} to L_α mesophase transitions, in the presence of either hydrophobic SiO_2 NPs (14 nm) or hydrophilic SiO_2 NPs (10 nm) at three different NP concentrations (*i.e.* NP-to-lipid number ratio of 10^{-6}, 10^{-5} and 10^{-4}). The overriding observation is that the H_{II}/L_α boundaries in the DOPE *p*–*T* phase diagram were shifted by the presence of NPs: the hydrophobic NPs enlarged the H_{II} phase region, whilst hydrophilic NPs appeared to stabilise the L_α phase region. This effect was also NP-concentration dependent, with a more pronounced effect for higher concentration of the hydrophobic NPs, but the trend was less clear cut for the hydrophilic NPs. As compared to the control sample without NPs, the presence of both types NPs generally enhanced the fluidity and reduced the compressibility of the lipid monolayers, with smaller *d*-spacing of the H_{II} and L_α phases. Thermodynamically, we have speculated that the effect of NPs on the mesophases transition derives from the balance between their interactions with the lipid headgroups and tails, and the volume change during the phase transition, according to the Clapeyron equation. Physically, we have proposed that the different effects of two different types of NPs on the mesophase transitions is a result of the balance between two factors: (1) the lipid–NP interactions dictated by the hydrophobicity of the particle surface; and (2) the elastic energy cost due to the mismatch between the equilibrium curvature of the mesophases and the local curvature of the NP-bound lipid monolayers and bilayers templated by the NPs.

The understanding of the interactions between NPs and mesophases at such thermodynamic and energetic levels, as facilitated by the rigorous and quantitative physicochemical techniques, in this case high pressure-SAXS, will add to our fundamental knowledge relevant to hybrid nanocomposites and cellular entrance by nanoparticles in the field of nanotoxicity and nanotheranostics.

Experimental

Sample preparation

1,2-Dioleoyl-*sn-glycero*-3-phosphoethanolamine (DOPE in chloroform, >99% purity) was purchased from Avanti Polar Lipids (Alabama, USA) and used as received. For the mesophase preparation, DOPE, stored at −30 °C, was allowed to warm to room temperature before the bottle was opened. Small volumes of lipid solution were transferred using a Pasteur pipette into glass vials and the chloroform was evaporated off inside a vacuum oven (Heraeus Vacutherm VT 6025) fitted with a acetone-dry ice cold trap at 1–30 mbar overnight at room temperature. Samples were then frozen in an acetone-dry ice bath at −78 °C and residual water was then removed in a freeze drier (Christ Alpha 1–2 LD plus). Approximately 10 mg of dried lipid was then weighed out into labelled glass vials for each sample.

Silica nanoparticles (SiO_2NPs) were either hydrophilic (PlasmaChem, Berlin, Germany Silicon Dioxide content >92.7%) or hydrophobic silica NPs (PlasmaChem; with polydimethylsiloxane coating). They had a nominal size of 10 and 14 nm respectively, although TEM images showed a size range of 10–15 nm for the hydrophilic silica nanoparticles and 14–19 nm for the hydrophobic ones (*cf.* Fig. S2 and S3 in the ESI†). The hydrophilic silica nanoparticles gave a zeta potential reading of ∼34.9 mV in water (ESI†). To add SiO_2 NPs to lipids, stock NP solutions (10 mg in MilliQ water for the hydrophilic NPs; and 10 mg in chloroform for the hydrophobic NPs) were first prepared. Then to each sample vial a certain volume of NP solution was added to give the required NP concentration (or NP/lipid number ratio, ν; see below). All samples were subsequently centrifuged at 5000 rpm for 30 minutes (Sigma 3-16PK), before being transferred to a plate shaker incubator (Stuart Microtitre) at room temperature (RT) for overnight shaking at 500 rpm to homogenise the lipid–NP mixture. The temperature of the shaker was increased to 40 °C and the samples were further agitated for 2 hours at 850 rpm. Chloroform was then removed from the mixture *in vacuo* (at RT and 10 mbar) and water was removed by freeze–drying. To further homogenise samples containing hydrophilic SiO_2NPs, ∼1 ml chloroform was added and the samples were shaken for another 2 hours at 40 °C, 850 rpm, before the chloroform was removed by the vacuum oven. To hydrate the dried lipid–NP mixtures to the designated water concentration (60% DOPE : 40% H_2O), MilliQ water (18.2 MΩ cm^{-1}) was added with an Eppendorf© pipette and the samples were centrifuged for 30 minutes at 5000 rpm followed by shaking in the incubator for 2 hours at 40 °C. Each sample was subjected to 12 freeze–thaw cycles by alternate submersion of the vials in an acetone-dry ice mixture (−78 °C) then warm water (∼40 °C). The samples were then stored in a freezer until the experiment and allowed to warm to RT before SAXS measurements.

High pressure SAXS (HP-SAXS)

SAXS was carried out at Beamline I22 at the Diamond Light Source utilising a high pressure system designed by Brooks *et al.*[50] The X-rays had an energy of 17 keV, corresponding to a wavelength of λ = 0.73 Å, with the shape of the beam approximately 300 by 250 μm (horizontal × vertical). A Pilatus2M high resolution (2 million pixel) area detector[51] was used to collect scattered X-rays from the samples. The sample to detector distance was 1.26 m, allowing a Q range from 0.01 $Å^{-1}$ to 2 $Å^{-1}$. An exposure time of 1 second was used throughout the experiment. Samples were enclosed in a sample holder consisting of a circular polytetrafluoroethylene (PTFE) washer with a 3 mm aperture sealed with Mylar film (50 μm in thickness) via double sided tape.[50] This sample holder had a volume of 11 mm^3. Once mounted and prior to SAXS measurements, the samples were subject to pressure cycling from 1 to 2600 bar five times to further homogenise the samples and also to check for sealing of the sample holder under high pressure. To construct the p–T phase diagrams (*cf.* Fig. 2 and 3 below), the pressure was varied hydrostatically from 0 to 3000 bar in 300 bar steps for a given temperature, which was itself varied from 20 to 45 °C in 5 °C steps. Samples were allowed 30 minutes to equilibrate after each temperature step and 2 minutes to equilibrate after each pressure step. After each pressure ramp at a given temperature, the sample was returned to ambient pressure and another SAXS image was taken, which was compared to the image taken before the pressure ramp, to check for radiation damage and to ensure the sample had not leaked. To further avoid radiation damage the sample was moved out of the beam as temperature was increased then returned to its measurement position after thermal equilibration. The sample position was also translated by approximately 300 μm between each temperature to minimise radiation damage.

Data Analysis

2D diffraction patterns were reduced to 1D curves using a YAX[52,53] macro in ImageJ. An image mask was generated to ensure that inactive parts of the detector were not included in the data reduction. The Q range of all the images was calibrated utilising that of AgBe standard (d-spacing 58.38 Å[54]) with a manual calibration function. The 2D diffraction patterns were then batch processed into text format. This file was then imported into Igor Pro© where peak positions, ratios of these peak positions and therefore the phase of the sample were determined along with the coherence length L of certain peaks utilising the built-in Multipeak Fitting 2.0 function. L is a measure of the size of the ordered domains that scatter coherently and contribute to the observed diffraction peaks in the case of a lamellar phase, and is calculated from the Scherrer equation,[48,55,56] $L = 2\pi K/\Delta Q$, where ΔQ is the full width at half maximum (FWHM) of the peak and K is a shape factor of order unity.

Acknowledgements

WHB acknowledges funding from the Engineering and Physical Science Research Council (EPSRC), the Royal Society and the European Research Council (ERC), Taiho Kogyo Tribology Research Foundation (TTRF); the European for Cooperation in Science and Technology (CMST COST) Action CM1101, and

the Marie Curie Initial Training Network (MC-ITN) NanoS3. JMB and BQ are supported by University of Bristol DTA studentships. TS is supported by an EPSRC CASE award and CB is supported by a CTD studentship *via* Bristol Centre for Functional Nanomaterials (BCFN). We also acknowledge Diamond Light Source for the award of beamtime under proposal SM6137.

References

1 J. C. Shah, Y. Sadhale and D. M. Chilukuri, *Adv. Drug Delivery Rev.*, 2001, **47**, 229–250.
2 K. Simons and W. L. C. Vaz, *Annu. Rev. Biophys. Biomol. Struct.*, 2004, **33**, 269–295.
3 S. Chesnoy and L. Huang, *Annu. Rev. Biophys. Biomol. Struct.*, 2000, **29**, 27–47.
4 I. Koltover, T. Salditt, J. O. Rädler and C. R. Safinya, *Science*, 1998, **281**, 78–81.
5 M. Rappolt, The biologically relevant lipid mesophases as ''seen'' by X-rays, in *Adv planar lipid bilayers and liposomes*, v5, ed. A. Liu, 2007.
6 J. Als-Nielsen and D. McMorrow, *Elements of mordern X-ray Physics*, Wiley, Chichester, 1st edn, 2001.
7 R. Mezzenga, C. Meyer, C. Servais, A. I. Romoscanu, L. Sagalowicz and R. C. Hayward, *Langmuir*, 2005, **21**, 3322–3333.
8 L. Sagalowicz, R. Mezzenga and M. E. Leser, *Curr. Opin. Colloid Interface Sci.*, 2006, **11**, 224–229.
9 S. Fraser, F. Separovic and A. Polyzos, *Eur. Biophys. J.*, 2009, **39**, 83–90.
10 R. Efrat, E. Kesselman, A. Aserin, N. Garti and D. Danino, *Langmuir*, 2009, **25**, 1316–1326.
11 R. Winter and C. Jeworrek, *Soft Matter*, 2009, **5**, 3157–3173.
12 B. Kent, C. J. Garvey, D. Cookson and G. Bryant, *Chem. Phys. Lipids*, 2009, **157**, 56–60.
13 F. Lopez-Garcia, J. Villalain, J. C. Gomez-Fernandez and P. J. Quinn, *Biophys. J.*, 1994, **66**, 1991–2004.
14 S. S. Funari, *Eur. Biophys. J.*, 1998, **27**, 590–594.
15 S. Aeffner, T. Reusch, B. Weinhausen and T. Salditt, *Eur. Phys. J. E: Soft Matter Biol. Phys.*, 2009, **30**, 205–214.
16 R. B. Thompson, V. V. Ginzburg, M. W. Matsen and A. C. Balazs, *Science*, 2001, **292**, 2469–2472.
17 B. Yuan, L.-L. Xing, Y.-D. Zhang, Y. Lu, Z.-H. Mai and M. Li, *J. Am. Chem. Soc.*, 2007, **129**, 11332–11333.
18 X. Chen, E. Shlomo, R. Oren, W. Wang, L. Niu, Z. Sui, B. Zhu, X. Yuan and K. Yang, *Sci. China, Ser. B: Chem.*, 2001, **44**, 492–499.
19 D. P. Siegel, *Biophys. J.*, 1999, **76**, 291–313.
20 C. M. Beddoes, C. P. Case and W. H. Briscoe, *Adv. Colloid Interface Sci.*, 2015, **218**, 48–68.
21 G. Oberdörster, E. Oberdörster and J. Oberdörster, *Environ. Health Perspect.*, 2005, 823–839.
22 H. C. Fischer and W. C. Chan, *Curr. Opin. Biotechnol.*, 2007, **18**, 565–571.
23 A. E. Nel, L. Mädler, D. Velegol, T. Xia, E. M. Hoek, P. Somasundaran, F. Klaessig, V. Castranova and M. Thompson, *Nat. Mater.*, 2009, **8**, 543–557.
24 C. Medina, M. Santos-Martinez, A. Radomski, O. Corrigan and M. Radomski, *Br. J. Pharmacol.*, 2007, **150**, 552–558.
25 H. F. Krug and P. Wick, *Angew. Chem., Int. Ed.*, 2011, **50**, 1260–1278.
26 G. A. Pilkington and W. H. Briscoe, *Adv. Colloid Interface Sci.*, 2012, **179**, 68–84.
27 J. Briggs, H. Chung and M. Caffrey, *J. Phys. II*, 1996, **6**, 723–751.
28 E. Y. Shalaev and P. L. Steponkus, *Biochim. Biophys. Acta, Bioenerg.*, 1999, **1419**, 229–247.
29 H. Qiu and M. Caffrey, *J. Phys. Chem. B*, 1998, **102**, 4819–4829.
30 A. M. Squires, C. E. Conn, J. M. Seddon and R. H. Templer, *Soft Matter*, 2009, **5**, 4773–4779.
31 J. M. Seddon, *Biochim. Biophys. Acta, Bioenerg.*, 1990, **1031**, 1–69.
32 H. Le Chatelier and O. Boudouard, *Bull. Soc. Chim. Fr.*, 1898, **19**, 483–488.
33 R. Winter, *Biochim. Biophys. Acta, Protein Struct. Mol. Enzymol.*, 2002, **1595**, 160–184.
34 M. Kozlov and M. Winterhalter, *J. Phys. II*, 1991, **1**, 1077–1084.
35 W. Helfrich, *Z. Naturforsch., C: J. Biosci.*, 1973, **28**, 693–703.
36 T. Y. D. Tang, A. M. Seddon, C. Jeworrek, R. Winter, O. Ces, J. M. Seddon and R. H. Templer, *Soft Matter*, 2014, **10**, 3009–3015.
37 N. J. Brooks, O. Ces, R. H. Templer and J. M. Seddon, *Chem. Phys. Lipids*, 2011, **164**, 89–98.
38 T. Y. D. Tang, N. J. Brooks, C. Jeworrek, O. Ces, N. J. Terrill, R. Winter, R. H. Templer and J. M. Seddon, *Langmuir*, 2012, **28**, 13018–13024.
39 J. N. Israelachvili, D. J. Mitchell and B. W. Ninham, *J. Chem. Soc., Faraday Trans.*, 1976, **72**, 1525–1568.
40 J. M. Seddon, A. M. Squires, C. E. Conn, O. Ces, A. J. Heron, X. Mulet, G. C. Shearman and R. H. Templer, *Philos. Trans. R. Soc., A*, 2006, **364**, 2635–2655.
41 K. Gawrisch, V. A. Parsegian, D. A. Hajduk, M. W. Tate, S. M. Gruner, N. L. Fuller and R. P. Rand, *Biochemistry*, 1992, **31**, 2856–2864.
42 Z. Chen and R. Rand, *Biophys. J.*, 1997, **73**, 267.
43 I. I. Slowing, J. L. Vivero-Escoto, C. W. Wu and V. S. Lin, *Adv. Drug Delivery Rev.*, 2008, **60**, 1278–1288.
44 W. Tan, K. Wang, X. He, X. J. Zhao, T. Drake, L. Wang and R. P. Bagwe, *Med. Res. Rev.*, 2004, **24**, 621–638.
45 I. Slowing, B. G. Trewyn and V. S. Y. Lin, *J. Am. Chem. Soc.*, 2006, **128**, 14792–14793.
46 L. C. J. Thomassen, A. Aerts, V. Rabolli, D. Lison, L. Gonzalez, M. Kirsch-Volders, D. Napierska, P. H. Hoet, C. E. A. Kirschhock and J. A. Martens, *Langmuir*, 2010, **26**, 328–335.
47 E. Venugopal, S. K. Bhat, J. J. Vallooran and R. Mezzenga, *Langmuir*, 2011, **27**, 9792–9800.
48 J. M. Bulpett, A. M. Collins, N. H. Kaus, P. T. Cresswell, O. Bikondoa, D. Walsh, S. Mann, S. A. Davis and W. H. Briscoe, *J. Mater. Chem.*, 2012, **22**, 15635–15643.
49 B. J. Reynwar, G. Illya, V. A. Harmandaris, M. M. Müller, K. Kremer and M. Deserno, *Nature*, 2007, **447**, 461–464.

50 N. J. Brooks, B. L. Gauthe, N. J. Terrill, S. E. Rogers, R. H. Templer, O. Ces and J. M. Seddon, *Rev. Sci. Instrum.*, 2010, **81**, 064103.
51 C. Brönnimann, R. Baur, E. Eikenberry, S. Kohout, M. Lindner, B. Schmitt and R. Horisberger, *Nucl. Instrum. Methods Phys. Res., Sect. A*, 2001, **465**, 235–239.
52 http://www.cunninglemon.com.
53 S. L. Gras and A. M. Squires, *Methods Mol. Biol.*, 2011, **752**, 147–163.
54 T. Huang, H. Toraya, T. Blanton and Y. Wu, *J. Appl. Crystallogr.*, 1993, **26**, 180–184.
55 A. Patterson, *Phys. Rev.*, 1939, **56**, 978.
56 T. G. Dane, P. T. Cresswell, O. Bikondoa, G. E. Newby, T. Arnold, C. F. Faul and W. H. Briscoe, *Soft Matter*, 2012, **8**, 2824–2832.